Monthly Notices of the ROYAL ASTRONOMICAL SOCIETY

MNRAS **504,** 3909–3921 (2021)
Advance Access publication 2021 April 16

doi:10.1093/mnras/stab1016

Dynamics of a superdense cluster of black holes and the formation of the Galactic supermassive black hole

P. Chassonnery[1,2]★ and R. Capuzzo-Dolcetta[2]★

[1]*Department of Mathematics, École Normale Supérieure Paris-Saclay, 61 Avenue du Président Wilson, F-94230 Cachan, France*
[2]*Department of Physics, Sapienza University of Rome, Piazzale Aldo Moro 5, I-00185 Rome, Italy*

Accepted 2021 April 9. Received 2021 April 1; in original form 2020 August 28

ABSTRACT

The centre of our Galaxy is known to host a massive compact object, Sgr A*, which is commonly considered as a supermassive black hole of $\sim 4 \times 10^6\,\mathrm{M}_\odot$. It is surrounded by a dense and massive nuclear star cluster, with a half-mass radius of about 5 pc and a mass larger than $10^7\,\mathrm{M}_\odot$. In this paper, we studied the evolutionary fate of a very dense cluster of intermediate-mass black holes, possible remnants of the dissipative orbital evolution of massive globular cluster hosts. We performed a set of high-precision *N*-body simulations taking into account deviations from pure Newtonian gravitational interaction via a post-Newtonian development up to 2.5 order, which is the one accounting for energy released by gravitational wave emission. The violent dynamics of the system leads to various successive merger events to grow a single object containing ∼25 per cent of the total cluster mass before partial dispersal of the cluster, and to generate, in different bursts, a significant quantity of gravitational wave emission. If generalized, the present results suggest a mechanism of mass growth up to the scale of a supermassive black hole.

Key words: methods: numerical – stars: black holes – Galaxy: centre – globular clusters: general – black hole mergers.

1 INTRODUCTION

Many galaxies, including our Milky Way, show evidence of the presence of a compact massive object (CMO) in their centres. These CMOs might be massive or even supermassive black holes (SMBHs) or be in the form of very massive and dense star clusters, commonly referred to as nuclear star clusters (NSCs). The actual 'direct' evidence of the presence of an SMBH has been recently given by the Event Horizon Telescope (EHT) that gave the first 'image' of the shadow produced by the event horizon of a BH of estimated mass of $6.5 \times 10^9\,\mathrm{M}_\odot$ in the centre of the giant elliptical galaxy M87 in the Virgo cluster (Event Horizon Telescope Collaboration 2019).

Unfortunately, so far, the EHT was not able to provide same evidence for the SMBH of about $4.3 \times 10^6\,\mathrm{M}_\odot$ (Gillessen et al. 2009) allegedly present in the centre of our Galaxy. This presence has been clearly suggested by the intense X-ray and radio emission and by the striking observation of the very rapid motion of a certain number of stars very close (within the central arcsec) to the Sgr A* radio source, as ascertained by two international groups, one at MPE in Garching (Gillessen et al. 2009; Schartmann, Burkert & Ballone 2018) and another one at UCLA (Ghez et al. 2005; Boehle et al. 2016). These stars, referred to as S-stars, have been studied over a period of time of about 18 yr. One of them, S2 in the denomination given by the MPE group, travelling on its highly eccentric orbit, reached its pericentre distance of about 120 au at a speed of $\sim 7650\,\mathrm{km\,s^{-1}}$ (2.55 per cent of the speed of light). Although 120 au is a very close approach (∼4 times the average Neptune's distance to the Sun and twice the Pluto orbit semimajor axis), it is still well apart from the hypothetical SMBH singularity (∼1400 Schwarzschild's radii of the hypothetical Sgr A* BH). According to GRAVITY Collaboration (2018), the observed gravitational redshift $z \sim 6.7 \times 10^{-4}$ confirms the motion in a regime of strong field. Later, GRAVITY Collaboration (2020) was able to pick another relativistic effect, namely the prograde precession of the S2 orbit pericentre angle. Anyway, it cannot in principle be excluded that this strong gravitational field at 120 au from the globular cluster (GC) is due to a superdense cluster of stars or, more likely, of compact objects.

The evolution of a very dense stellar system is a quite intriguing and non-trivial issue. Pioneering work in such field was done by Spitzer & Saslaw (1966) and Spitzer & Stone (1967) although in a necessarily approximate scheme due to the poor computer resources at that time. They found that, unless the stellar system has enough angular momentum to inhibit its contraction at a relatively low stellar density, the process of accelerating contraction of its core must lead inevitably to an increasing number of collisions between the stars in the cluster. Consequently, all stellar aggregations with sufficiently low angular momentum would reach a stage in which direct stellar collisions play a dominant role in the further evolution of the system itself. However, the situation of a cluster of compact objects (white dwarves, neutron stars, and BHs) would be different because no significant physical collisions would occur to release gas that cools down in the environment possibly giving rise to new stars. So, while the initial phase of core contraction and halo expansion should be similar, the following evolutionary phases of a dense system of normal stars and one composed of compact remnants are likely very different.

★ E-mail: pauline.chassonnery@ens-cachan.fr (PC); roberto.capuzzodolcetta@uniroma1.it (RCD)

Such a scheme was later deepened by Lightman & Fall (1978), who gave an approximate theory of evolution towards core collapse of a cluster composed of stars of two different masses. At this latter regard, it is worth also citing Begelman & Rees (1978). Their qualitative conclusion is that a system composed solely of compact stellar mass bodies would evolve at constant binding energy until a small fraction of the original mass developed into a relativistic bound core, where the physics is of course different and phenomena like energy release by gravitational waves (GWs) and subsequent merger phenomena cannot be neglected and require a sophisticated treatment.

The classical computation of the two-body collision relaxation time-scale (Spitzer & Hart 1971) gives for the hypothetical cluster of 400 intermediate-mass black holes (IMBHs) initially packed in a 0.6 mpc sphere a value of the fraction of 1 yr. Although this very short time-scale suggests that the superviolent evolution of the system would lead through a sudden instability to a probable disgregation of the system, much care is due to that the deduction of the relaxation time-scale bases on the evaluation of diffusion coefficients in the weak scattering regime and, of course, neglecting any relativistic effects. Both these hypotheses are not realized in the real evolution of a dense system of IMBHs, which seems, so, an interesting theme to investigate.

Kroupa et al. (2020) provide a modern vision of the fate of a compact cluster of stellar-size BHs left over by the evolution of the stellar population originated in starburst clusters residing in the central region of a galaxy shortly after its formation. Their main finding, based on a modelization that privileges a global view of various evolutionary ingredients with respect to accurate *N*-body modelling in both Newtonian and post-Newtonian (PN) phases, is that the BH cluster compresses down to a relativistic state (velocity dispersion of $\sim$3000 km s^{-1}) due to insufficient heating by forming BH–BH binaries. The onset of GW emission implies a loss of mechanical energy, which eventually leads to a runaway formation of an SMBH seed, with a 5 per cent of mass converted into the seed.

A somewhat similar result was obtained, still in a scheme that does not include direct *N*-body simulations, by Antonini, Gieles & Gualandris (2019), who investigate the BH repeated mergers in a dense star cluster ($\rho \gtrsim 10^5\,\mathrm{M_\odot}$, $v_{\rm esc} \gtrsim 300$ km s^{-1}, conditions fulfilled by $\sim$10 per cent of present-day NSCs) eventually leading to a very massive 'remnant' BH. Although upon different approximations and with different methods of study, both Antonini et al. (2019) and Kroupa et al. (2020) agree on that binary heating is insufficient, at least in a wide range of conditions, to support a cluster of stellar-size BHs against collapse.

In the above context, the well-known dry-merger scenario for the building up of NSCs (Tremaine, Ostriker & Spitzer 1975; Capuzzo-Dolcetta 1993; Antonini et al. 2012) suggests that orbitally decayed massive GCs have carried to the Galactic Centre a quantity of mass to grow the NSC of the Milky Way and also a certain number of IMBHs. So, the aim of this paper is the study of the evolutionary fate of a possible superdense cluster, composed of 400 IMBHs of individual mass $10^4\,\mathrm{M_\odot}$, initially packed in a sphere well within the S2 pericentre distance. Our work represents a significant step forward after the Kupi, Amaro-Seoane & Spurzem (2006) paper that studied the dynamics of a dense cluster of compact objects by means of a modified version of the NBODY6++ code (Aarseth 1999; Spurzem 1999) to allow for PN effects up to order 2.5.

The paper is organized as follows: In Section 2, the astrophysical frame and the motivations are explained. In Section 3, we describe our methodological approach and the kind of numerical simulations we performed, while in Section 4 we discuss the results. Finally, in Section 5 we draw the conclusions.

2 THE ASTROPHYSICAL FRAMEWORK

Massive and sufficiently compact objects can decay orbitally in a stellar environment due to the drag caused by the 'wake' they form behind them during their motion. This is the well-known 'dynamical friction' (df) phenomenon, whose study was pioneered by Chandrasekhar (1943). In particular, it has been convincingly shown that massive GCs orbiting a galaxy like the Milky Way might decay in the inner region of the host galaxy whenever their orbits are eccentric enough to pass, during their travel across the galaxy, through regions where the environmental phase-space density, whose proxy is ρ/σ^3 (with ρ and σ the local mass density and velocity dispersion, respectively), is high enough to induce a significant deceleration.

Actually, the dynamical friction orbital decay has been considered by various authors as a viable explanation for the formation of the NSCs present in our and other galaxies. The so-called *migratory* scenario consists in the orbital decay of a certain number of massive star clusters, followed by their merger in the central region of the galactic potential well. This scenario has been quantitatively validated by many papers (Tremaine et al. 1975; Ostriker, Binney & Saha 1989; Pesce, Capuzzo-Dolcetta & Vietri 1992; Capuzzo-Dolcetta 1993; Capuzzo-Dolcetta & Vicari 2005; Arca-Sedda & Capuzzo-Dolcetta 2014a, b). Here, we assume this scenario, which is alternative and/or complementary to the '*in situ*' model (see e.g. Agarwal & Milosavljević 2011), to motivate our choice of initial conditions for our evolutionary model. We do not go here into further details, pointing the attention to the recent review on NSCs by Neumayer, Seth & Böker (2020).

The hypothesis behind our work is that a certain number of massive star clusters (hereafter referred to as GCs) containing one or few IMBHs whose mass ranges between few $10^3\,\mathrm{M_\odot}$ and few $10^4\,\mathrm{M_\odot}$ have had the time to decay orbitally in an internal region of the host galaxy, carrying with them the hosted IMBHs. The actual presence of such IMBHs, although not clearly confirmed so far by present observations of GCs in the MW halo, would result as a natural interpolation of the host mass versus hosted BH mass correlation over the wide range of scales from open star clusters up to giant elliptical galaxies (see Fig. 1).

For the BH mass versus host mass, Schutte, Reines & Greene (2019) provide (their equation 11; see also Fig. 1) the following fitting formula:

$$\mathrm{Log}(M_{\rm BH}/\mathrm{M_\odot}) = \alpha + \beta \mathrm{Log}(M_{\rm bulge,*}/(10^{11}\,\mathrm{M_\odot})), \tag{1}$$

with $\alpha = 8.80 \pm 0.085$ and $\beta = 1.24 \pm 0.081$.

As we said, an enormous quantity of papers has been dedicated to the topic of the dynamical friction decay time for massive objects, which surely we do not review here, limiting to cite that dynamical friction is, of course, more efficient on massive objects moving on *centrophilic* orbits, which are numerous in non-symmetric galactic potentials whose typical example is the triaxial case. Pesce et al. (1992) showed how efficient dynamical friction can be to brake massive clusters in triaxial galaxies, even of moderate axial ratios (1:1.25:2). That work was extended and deepened by Capuzzo-Dolcetta (1993), who gave two useful interpolation formulas for the df decay time of a compact cluster moving on both *box* or *loop* orbits in a triaxial potential. Using formulas A1, A2, and A3 of Capuzzo-Dolcetta (1993), we computed dynamical friction decay time as functions of orbital energy ($0 \le E \le 1$, $E = 1$ is the threshold to unbound orbits) and angular momentum scaled to that of circular obit of energy E, $J/J_c(E)$. Upon this, we draw Fig. 2, which shows the dynamical friction times as a function of the cluster orbital energy and

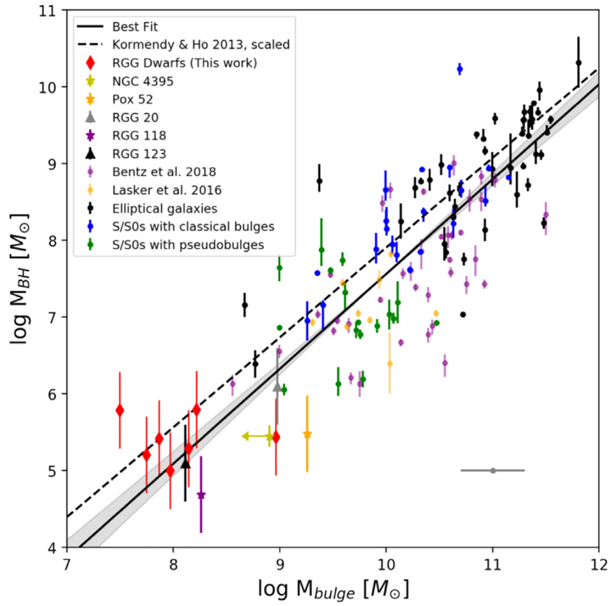

Figure 1. BH mass versus host bulge mass (from Schutte et al. 2019, Fig. 4).

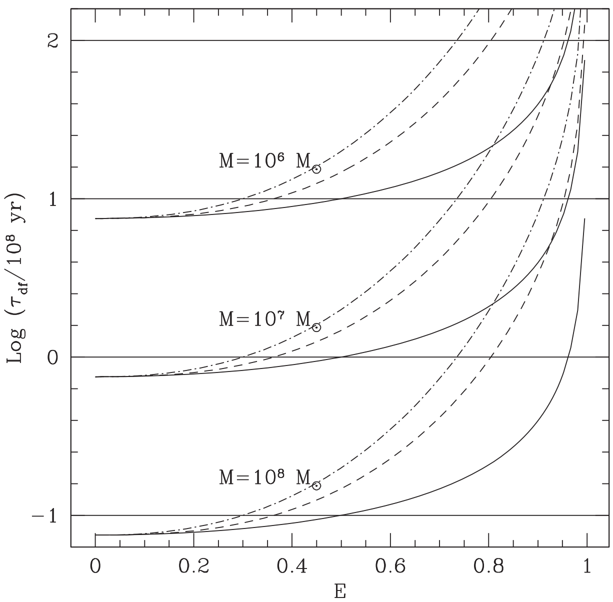

Figure 2. Dynamical friction decay times at varying the object mass M for three values of $J/J_c(E)$ (0, 0.5, and 1; solid, dashed and dot-dashed line, respectively) as a function of the orbital energy E. Horizontal lines give the 10^7, 10^8, 10^9, and 10^{10} yr thresholds.

angular momentum. Almost all GCs with masses larger than 10^7 M$_\odot$ would have decayed to the central region of the host galaxy within 1 Gyr. Additionally, an extrapolation of the fitting formula given by equation (1) gives, for a hypothetical 10^4 M$_\odot$ BH, a host mass of 1.35×10^7 M$_\odot$. This means that, if these massive GCs hosted IMBHs at their centre, in less than 1 Gyr they should have carried them to the galactic central region.

In this frame, we took 10^4 M$_\odot$ as individual IMBH mass and decided to study the dynamical evolution of a system of $N_{\rm BH} = 400$ BHs, whose summed mass is almost equal, indeed, to the estimated Sgr A* mass, considering them as all initially packed within the innermost pericentre distance of the S stars moving around it, that is $\simeq$0.6 mpc. This initial configuration is the simplest to adopt, although not the most likely one. Actually, a more reasonable frame would be that where the various GC hosts of the IMBHs shrink their orbit within an assumed galactocentric distance at different times. This frame is more difficult to implement numerically and so its study is postponed to a following paper.

3 MODEL AND METHOD

The above-mentioned very dense cluster of IMBHs is expected to be extremely prone to instability to collapse, because its two-body classical relaxation time-scale is of the order of (or less than) 10 yr, which is of course a very short time with respect to all other relevant time scales. Anyway, considerations on the instability of a very dense cluster based on the classical evaluation of the two-body relaxation time-scale have to be taken with care because, other than that the usual expression of the time-scale bases on the unlikely hypothesis that two-body interactions are weak, they do not account for the possible support against collapse given by binarity. In this regard, Kroupa et al. (2020) suggest that BH–BH binary heating can be overcome by the huge compression of the BH population inhabiting a massive starburst cluster due to the gas accretion from the environment. So, although the likely fate of our hypothetical superdense cluster is that of a gravitational collapse, its actual modes are not trivial to understand, including the number of mergers and of expelled IMBHs, binary fraction and its evolution along the way as well as the possible runaway formation of an SMBH. Recently, Antonini et al. (2019) deduced a theoretical correlation between the maximum BH mass formed by repeated merger in a dense stellar system and the system characteristics. Dense clusters (density $\gtrsim 10^5$ M$_\odot$ pc^{-3} and escape velocity $\gtrsim$300 km s^{-1}) lead to BH merger mass of up to 10^5 M$_\odot$, filling the pair instability strip. This should have relevant counterpart in GW emission and detection.

Due to the intrinsic non-linearity of the violent dynamical evolution of the cluster, analytical or semi-analytical treatments fail to give precise answers to the many questions that arise, and so we decided to study the evolution of the above-mentioned very dense cluster of IMBHs by a direct, high-precision, N-body approach. The mutual accelerations induced by point-like mass objects packed in a small region of space are so strong that any 'classic' integration algorithm fails due to the *UV* divergence of the Newtonian potential. To overcome this problem, we resorted to a high-accuracy, regularized code that is our modified version of the algorithmic regularization chain code by Mikkola (Mikkola & Merritt 2008; Hellström & Mikkola 2010). The code, called ARWV, and a user manual for it (Chassonnery, Capuzzo-Dolcetta & Mikkola 2019) are freely available to download at https://sites.google.com/uniroma1.it/astrogroup/hpc-html (the code can be used for scientific publications upon the proper citation condition).

The equations of motions of our set of N objects are (for $i = 1, 2, ..., N$)

$$\ddot{\mathbf{r}}_i = G \sum_{\substack{j=1 \\ j\neq i}}^{N} m_j \frac{\mathbf{r}_j - \mathbf{r}_i}{|\mathbf{r}_j - \mathbf{r}_i|^3} + \mathbf{f}_{\rm PN} + \nabla U_{\rm ext} + \mathbf{f}_{\rm df}. \quad (2)$$

In the formula above, G is the Newton's gravitational constant, $\mathbf{r}_i$ is the position vector of the generic ith object of mass m_i, $\mathbf{f}_{\rm PN}(\mathbf{r}_i, \mathbf{v}_i)$ is the PN force per unit mass, $\nabla U_{\rm ext}(\mathbf{r}_i)$ is the gradient of the external potential, and $\mathbf{f}_{\rm df}(\mathbf{r}_i, \mathbf{v}_i)$ is the dynamical friction force per unit mass.

The Newtonian self-interaction is evaluated via a direct summation of all pair contributions in equation (2), which implies a computational cost $\mathcal{O}(N^2)$, that limits the use of such kind of high-precision codes to a limited number of objects. Another limitation is given, also, by the *UV* divergence of the Newtonian potential, which makes extremely delicate, on the computational side, dealing with close encounters of massive objects, whose relative acceleration grows enormously at smaller separations. An accurate and elegant, but still computationally expensive way to deal with those close encounters is via *regularization* of the interaction, which is done by means of a combination of different techniques [i.e. using (i) logarithmic Hamiltonian (Mikkola & Tanikawa 1999a, b), (ii) time-transformed leapfrog (Mikkola & Aarseth 2002), and (iii) auxiliary velocity algorithm (Hellström & Mikkola 2010)].

The PN force in equation (2) is an actual approximation, as expansion in terms of the ratio $(v/c)^2$, to account for general relativistic correction to classic Newton's law of gravitation. The PN approximation was introduced by Einstein, Droste, and De Sitter just after the publication (in 1916) of the general theory of relativity. The reference paper is de Sitter (1916) and a proper summary of PN treatment is found in Merritt (2013). Of course, in the limit $(v/c)^2 < <1$ the pure Newtonian interaction is recovered. In $\mathbf{f}_{\rm PN}$ we consider PN terms up to the 2.5 orders, i.e. including $\mathcal{O}[(v/c)^2]^{5/2}$ terms, which are the ones needed to account for energy losses via gravitational radiation (Merritt 2013). We refer to Memmesheimer, Gopakumar & Schäfer (2004) for the detailed expressions and to Mikkola & Merritt (2008) for a description of the actual implementation in the code used here.

Taking into account that GR does not produce 0.5PN or 1.5PN contributions to the metric or the equations of motion, the PN force per unit mass acting on the ith particle is expressed by

$$\mathbf{f}_{\rm PN}(\mathbf{r}_i, \mathbf{v}_i) = c^{-2}\mathbf{f}_{\rm 1PN} + c^{-4}\mathbf{f}_{\rm 2PN} + c^{-5}\mathbf{f}_{\rm 2.5PN} + \mathcal{O}(c^{-6}). \tag{3}$$

Note that 1PN and 2PN terms ($\mathbf{f}_{\rm 1PN}$ and $\mathbf{f}_{\rm 2PN}$) are responsible for pericentre angular shift and are not dissipative (they are symmetric under time reflection $t \rightarrow -t$), while the first dissipative term (*radiation-reaction*) is the 2.5PN term ($\mathbf{f}_{\rm 2.5PN}$), which is indeed antisymmetric under time reflection.

The 2.5PN terms (radiation-reaction terms) are responsible for the GW emission that extracts mechanical energy from the systems at every merger occurrence. This corresponds to some variation of the mass after merger. We a posteriori saw that the quantity of energy lost via GW corresponds to a loss of mass <0.05 per cent of the total mass in all our simulation sets (see Section 4.3), a quantity small enough to justify keeping the mass of individual objects in our simulations unchanged.

Our updated version of ARWV also includes a treatment of an external gravity field in spherical symmetry, due to the presence of a regular distribution of matter in the form of a Dehnen (1993) profile and/or a Plummer (1911) profile. A Dehnen (or γ) density profile is univoquely defined by its total mass $M_{\rm D}$, scale radius $r_{\rm D}$, and slope parameter $0 \leq \gamma < 3$, while a Plummer profile is characterized by its total mass $M_{\rm P}$ and scale radius $r_{\rm P}$ only. The role played by the overall, regular, density distribution is that of giving both an additional gravitational acceleration to the point-like objects and a frictional braking, mimicking the cumulative, fluctuating, role of the encounters, via the dynamical friction term, $\mathbf{f}_{\rm df}$, in the equations of motion (equation 2), which is generally accounted for by means of the usual Chandrasekhar's expression in local approximation (Chandrasekhar 1943):

$$\mathbf{f}_{\rm df}(\mathbf{r}, \mathbf{v}) = -4\pi G^2 \ln\Lambda\, m\, \rho(\mathbf{r}) F(v/\sigma)\, \frac{\mathbf{v}}{v^3}, \tag{4}$$

where $\ln\Lambda$ is the Coulomb logarithm (here assumed =6.5), m is the mass of the 'test' particle, $\rho(\mathbf{r})$ is the local mass density of the field whose 3D velocity dispersion is σ, and $\mathbf{v}$ is the velocity of the 'test' particle. The function $F(v/\sigma)$ is given by

$$F(v/\sigma) = \mathrm{erf}\left(\frac{v/\sigma}{\sqrt{2}}\right) - \sqrt{\frac{2}{\pi}}\frac{v}{\sigma}\mathrm{e}^{-\frac{1}{2}(v/\sigma)^2}, \tag{5}$$

where erf(x) is the usual error function, defined as

$$\mathrm{erf}(x) = \frac{2}{\sqrt{\pi}}\int_0^x \mathrm{e}^{-t^2}\,\mathrm{d}t \leq 1. \tag{6}$$

The central environment of the Milky Way can be emulated by a superposition of a Dehnen profile and a Plummer profile, characterized, respectively, by the sets of values $M_{\rm D} = 10^{11}\,\mathrm{M}_\odot$, $r_{\rm D} = 2000$ pc, $\gamma_{\rm D} = 0.1$ (Arca-Sedda & Capuzzo-Dolcetta 2017) and $M_{\rm P} = 2.5 \times 10^7\,\mathrm{M}_\odot$, $r_{\rm P} = 3.2$ pc (to give the NSC mass and half-light radius as given by Schödel et al. 2014). As it will be shown in Section 3.3, for the peculiar initial conditions in study for this article, the actual effects of the external regular distributions of matter (both gravitational acceleration and dynamical friction) are negligible.

Let us now give some information about the ARWV code. Usually, after assuming an arbitrary indexing of the N bodies from 1 to N, the position and velocity of each body with respect to the centre of mass (CoM) of the system are stored in an array of size 6N. In ARWV, the first body, arbitrarily chosen, is considered as a temporary 'reference' point and the other bodies are renumbered so as to minimize the distance between the ith and $(i+1)$th objects ($i = 1, 2, ..., N-1$). With this new numbering, the bodies can be seen as forming a 'chain' connecting closest to closest body and can be described by their position and velocity, not with respect to the CoM of the system, but with respect to the previous (in terms of the chain numbering) body. These 'chain' data are stored in an array of size $6(N-1)$ (the first body, being the origin of the chain, is not referenced).

In practice, while creating the chain, the algorithm also tries to minimize the sum of the distance between two successive bodies so as to not inconveniently 'forget' any object, which would then have to be added at the end of the chain with an enormous distance to the penultimate object.

The main advantage of this chain scheme resides in that it reduces substantially the round-off errors, making the regularization algorithm more efficient, especially for close interactions between the system bodies. Without this formulation, the step size would reduce to almost zero in critical (very close) encounters. Its downfall is that the interactions are formally much more complicated.

3.1 Mergers and merger consequences

During the evolution of an N-body system, repeated interactions may lead to the formation of *binaries* (two bodies orbiting one around the other), which may be either temporary or long-living. If long-living, a binary composed of massive objects can eventually merge, losing, first, orbital energy by means of the interaction with the other bodies and, once the binary is tight enough, by means of gravitational radiation that, in our simulations, is accounted for by the 2.5PN terms. When speaking of massive BHs, this frame is surely important and likely, and needs to be properly accounted for when aiming at a correct simulation of their dynamics. In our ARWV code, there is indeed a *merger* routine that enables the code to deal with collisions. The procedure triggers when the distance r_{ij} between two objects of masses m_i and m_j is less than 4 times the sum of their Schwarzschild's radii, that is $r_{ij} \leq 8G(m_i + m_j)/c^2$.

To the result of the merger (the *remnant*) is given the location of the CoM of the progenitor pair, though the code halts the integration of the two separate trajectories immediately before that time. For the correct velocity to assign to the remnant (the recoil velocity), there is no consensus. Some authors choose the simplest (but clearly incorrect) choice to give to the remnant a null velocity, while others assume the velocity of the CoM of the two progenitors. In our new version of the ARWV code, we introduced a relativistic, spin-dependent, recoil velocity, following the prescription given by Healy & Lousto (2018). We shortly describe here the way we did it.

Let m_1 and m_2 be the masses of two merging bodies, with the convention $m_1 \leq m_2$. Each body is assumed to be spinning; the spin is characterized by a dimensionless spin vector parameter $\boldsymbol{\alpha}_i$, such that $\alpha_i \leq 1$.

Following Healy, Lousto & Zlochower (2014) and Healy & Lousto (2018), we model the recoil velocity by

$$\mathbf{v}_{\rm rec} = v_m\,\mathbf{e}_1 + v_\perp\,(\cos\xi\,\mathbf{e}_1 + \sin\xi\,\mathbf{e}_2)\,, \tag{7}$$

where $\mathbf{e}_1$ is the unit vector pointing from m_1 to m_2 and $\mathbf{e}_2$ a unit vector in the orbital plane and orthogonal to $\mathbf{e}_1$, such that the basis formed by $\mathbf{e}_1$, $\mathbf{e}_2$, and the angular momentum of the binary (that is, the mass-weighted sum of the angular momentum vectors of the two progenitor objects) is direct. The quantity ξ is the angle between the 'unequal' mass contribution to recoil velocity, whose magnitude is v_m, and the spin contribution, of magnitude $v_\perp$. While both ξ and $v_\perp$ depend on the values of the spins and of the mass ratio $0 < q = m_1/m_2 \leq 1$ (see Healy & Lousto (2018)), v_m depends only on q, in the following form:

$$v_m = \frac{q^2(q-1)}{(q+1)^5}\left[A + B\left(\frac{q-1}{q+1}\right)^2 + C\left(\frac{q-1}{q+1}\right)^4\right], \tag{8}$$

where $A = -8712$, $B = -6516$, and $C = 3907$, all in km s^{-1} (Healy, Lousto & Zlochower 2017; Healy & Lousto 2018).

Fig. 3 displays the dependence of v_m, $v_\perp$, and $v_{\rm rec}$ on the mass ratio q. Since $v_\perp$ and ξ (and so $v_{\rm rec}$) depend on the dimensionless spins $\boldsymbol{\alpha}_1$ and $\boldsymbol{\alpha}_2$, we chose to compute their average values with respect to these parameters. We made a regular sampling of the magnitudes α_1 and α_2 over [0, 1] with a step 0.01, and we took each dimensionless spin as being either 'up' (i.e. aligned with the angular momentum of the binary) or 'down' (i.e. antialigned). Then, we averaged the values of $v_\perp$ and $v_{\rm rec}$ obtained for each quadruple $[\alpha_1, \text{up/down}(\boldsymbol{\alpha}_1), \alpha_2, \text{up/down}(\boldsymbol{\alpha}_2)]$.

By its definition, the angle ξ depends on both the mass ratio and the spins. However, averaging over the uniform spin distribution the dependence on q is lost, leading to $\langle\xi\rangle_{\boldsymbol{\alpha}} = 142.6^\circ$.

We observe that v_m is maximal for $q \simeq 0.35$, with a nearly linear decrease for $q \geq 0.5$, while $v_\perp$ is roughly constant for high mass ratios and so becomes the preponderant part of $v_{\rm rec}$, which maximizes at $q \simeq 0.41$. The maximal recoil velocity over all the cases computed was obtained for maximally anti-aligned spins, and it is of the order of 500 km s^{-1} (see bottom panel of Fig. 3).

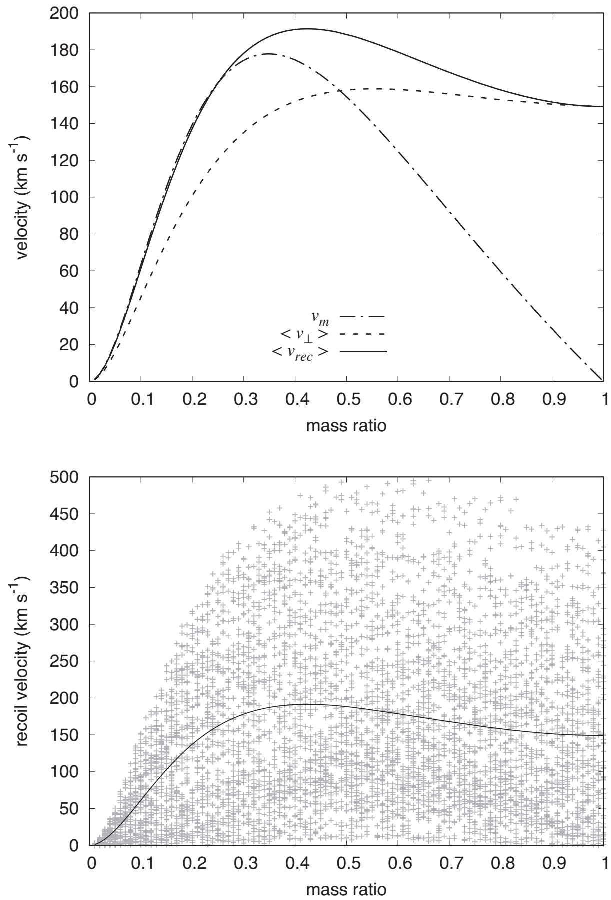

Figure 3. Top panel: variation with respect to the mass ratio (q) of v_m, $v_\perp$, and $v_{\rm rec}$, the latter two averaged over spin (see the text). Bottom panel: distribution of the recoil velocity magnitude $v_{\rm rec}$ (grey crosses) versus mass ratio, along with its average value (black line).

Table 1. Parameters characterizing the two (generic) merging objects m_1 and m_2.

	Before merger (t_m^-)	After merger (t_m^+)
Mass	m_1 and m_2	$m_{\rm rem} = m_1 + m_2$
Position	$\mathbf{r}_1$ and $\mathbf{r}_2$	$\mathbf{r}_{\rm rem} = \mathbf{r}_{\rm CoM}$
Velocity	$\mathbf{v}_1$ and $\mathbf{v}_2$	$\mathbf{v}_{\rm rem} = \mathbf{v}_{\rm CoM} + \mathbf{v}_{\rm rec}$
Spin	$\boldsymbol{\alpha}_1$ and $\boldsymbol{\alpha}_2$	$\boldsymbol{\alpha}_{\rm rem} = \frac{m_1\boldsymbol{\alpha}_1 + m_2\boldsymbol{\alpha}_1}{m_1+m_2}$

3.2 Energy variation at merger

Let us consider a merger between two bodies out of N (arbitrarily numbered 1 and 2) happening at time t_m, with $t_{\rm m}^-$ and $t_{\rm m}^+$ referring to a time just before and after merger, respectively. For all the bodies save the two undergoing a merger, we have

$$\begin{cases} m_i(t_{\rm m}^-) = m_i(t_{\rm m}^+), \\ \mathbf{r}_i(t_{\rm m}^-) = \mathbf{r}_i(t_{\rm m}^+), \\ \mathbf{v}_i(t_{\rm m}^-) = \mathbf{v}_i(t_{\rm m}^+), \end{cases} \tag{9}$$

while for the two merging bodies, the situation is resumed in Table 1.

Throughout the merger routine, the variation of the kinetic energy, T, of the system is

$$\begin{aligned} \Delta T(t_m) &= T(t_m^+) - T(t_m^-) \\ &= \frac{1}{2}\left(m_{\rm rm}\mathbf{v}_{\rm rm}^2 - m_1\mathbf{v}_1^2 - m_2\mathbf{v}_2^2\right) \\ &= \frac{m_{\rm rm}}{2}\left(v_{\rm rec}^2 + 2\mathbf{v}_{\rm rec}\cdot\mathbf{v}_{\rm CoM}\right) - \frac{m_1}{2}\tilde{v}_1^2 - \frac{m_2}{2}\tilde{v}_2^2, \end{aligned}$$

where the dot $\cdot$ indicates the scalar product, $\tilde{\mathbf{v}}_1 = \mathbf{v}_1 - \mathbf{v}_{\rm CoM}$, and $\tilde{\mathbf{v}}_2 = \mathbf{v}_2 - \mathbf{v}_{\rm CoM}$. On the other side, the variation of the internal potential energy (that of the pair) is

$$\begin{aligned}\Delta\Omega_{\rm int}(t_m) &= \Omega_{\rm int}(t_m^+) - \Omega_{\rm int}(t_m^-),\\ &= -\sum_{j=3}^{N}\frac{Gm_{\rm rm}m_j}{|\mathbf{r}_{\rm rm}-\mathbf{r}_j|} + \frac{Gm_1m_2}{|\mathbf{r}_1-\mathbf{r}_2|} + \sum_{i=1,2}\sum_{j=3}^{N}\frac{Gm_im_j}{|\mathbf{r}_i-\mathbf{r}_j|},\\ &\simeq -\sum_{j=3}^{N}\frac{Gm_{\rm rm}m_j}{|\mathbf{r}_{\rm rm}-\mathbf{r}_j|} + \frac{Gm_1m_2}{|\mathbf{r}_1-\mathbf{r}_2|} + \sum_{i=1,2}\sum_{j=3}^{N}\frac{Gm_im_j}{|\mathbf{r}_{\rm rm}-\mathbf{r}_j|},\\ &\simeq \frac{Gm_1m_2}{|\mathbf{r}_1-\mathbf{r}_2|},\end{aligned}$$

considering that, for any pair (i, j) with $i = 1, 2$ and $j \in \{3, ..., N\}$, we have $\tilde{r}_i \equiv |\mathbf{r}_i - \mathbf{r}_{\rm CoM}| \ll |\mathbf{r}_{\rm CoM} - \mathbf{r}_j|$, and so $|\mathbf{r}_i - \mathbf{r}_j| \simeq |\mathbf{r}_{\rm CoM} - \mathbf{r}_j| = |\mathbf{r}_{\rm rm} - \mathbf{r}_j|$. Finally, the variation of the external potential energy is

$$\begin{aligned}\Delta\Omega_{\rm ext}(t_m) &= \Omega_{\rm ext}(t_m^+) - \Omega_{\rm ext}(t_m^-),\\ &= -m_{\rm rm}U_{\rm ext}(\mathbf{r}_{\rm rm}) + m_1U_{\rm ext}(\mathbf{r}_1) + m_2U_{\rm ext}(\mathbf{r}_2),\\ &= \mathcal{O}\left((\tilde{r}_1^2 + \tilde{r}_2^2)\,\sup(U''_{\rm ext})\right).\end{aligned}$$

Given the above considerations, the total variation of the mechanical energy of the N-body system during the merging process is

$$\Delta E(t_m) \simeq \frac{m_{\rm rm}}{2}v_{\rm rec}^2 + m_{\rm rm}\mathbf{v}_{\rm rec}\cdot\mathbf{v}_{\rm CoM} - E_{\rm b}, \tag{10}$$

with $E_{\rm b} = \frac{m_1}{2}\tilde{v}_1^2 + \frac{m_2}{2}\tilde{v}_2^2 - \frac{Gm_1m_2}{|\mathbf{r}_1-\mathbf{r}_2|}$ the internal energy of the progenitor pair, which is negative in the case of a bound binary. So, neglecting the term $\mathbf{v}_{\rm rec}\cdot\mathbf{v}_{\rm CoM}$ that, on average over numerous merger events, should be null, we found that $\sum_{i\geq 1}\Delta E(t_m^i) > 0$.

3.3 Initial conditions

As we said above, our aim is that of simulating an extremely dense stellar cluster that could be a precursor of the Milky Way central SMBH. As total mass of our system we assumed $M_{\rm S} = 4\times10^6\,{\rm M}_\odot$, composed of $N = 400$ IMBHs of same individual mass $m = 10^4\,{\rm M}_\odot$.

The initial homogeneous and virialized very packed configuration was motivated by willing to verify how unstable such distribution was. Actually, a possible question could have been: Is it possible that a superdense system of gravitating objects distributed around the Galactic Centre lives long enough to make the surrounding S-stars moving as they are presently seen without invoking the presence of a BH singularity? Answering to this question with a full N-body simulation requires, indeed, 'packing' the 400 IMBHs in a sphere of initial radius, R_0, sufficiently smaller than the smallest pericentre of the S-stars (note that the innermost pericentres of the S-stars, those of S2 and S14, are about 5 mpc, where 1 mpc = 1 milliparsec = 10^{-3} pc).

A first set of simulations (hereafter referred to as set 1) was conducted with $R_0 = 0.6$ mpc, that is ∼10 times less than the smallest S-star pericentre distance. Under these quite extreme conditions ($\rho_0 \sim 4.4\times10^{15}\,{\rm M}_\odot\ {\rm pc}^{-3}$!), the cluster is expected to undergo a fast dynamical instability, so that, also for the sake of comparison, we run a second set of simulations (called set 2) with a 10 times larger initial radial size, $R_0 = 6$ mpc (same size of closest S-star pericentre distance). In the hypothesis of uniform spatial distribution, the central escape velocity in set 1 and set 2 is, respectively, $v_{\rm e,1} \simeq 7.11\times10^3$ and 2.25×10^3 km s^{-1}.

Table 2. Main parameters of the various sets of simulations. $t_{\rm max}$ is the maximum time extension of the simulation.

Set	R_0 (mpc)	$t_{\rm max}$ (yr)	Spin
1A	0.6	426	Zero
1B	0.6	426	Uniform
2A	6	13 462	Zero
2B	6	13 462	Uniform

As we said, the distribution of the initial positions ($\mathbf{r}_i$, for $i = 1, 2, ..., N$) of the $N = 400$ IMBHs has been assumed uniform within R_0, practically obtained by a standard pick-and-reject method.

The initial velocity distribution ($\mathbf{v}_i$, for $i = 1, 2, ..., N$) was assumed, also, randomly generated according to a uniform isotropic distribution scaled such as to give a chosen initial virial ratio $Q_0 \equiv 2T_0/|\Omega_0| = 1$ (where T and Ω are the total kinetic and potential energy, respectively).

To give some statistical reliability to our dynamical experiments, we have performed a total of 40 simulations with different sampling of the same initial conditions. Practically, for both set 1 and set 2 we generated 10 input files using the same global parameters ($N = 400$, $M_{\rm S} = 4\times10^6\,{\rm M}_\odot$, $R_0 = 0.6$ mpc for set 1, and $R_0 = 6$ mpc for set 2) but choosing different random seeds to sample the same (homogeneous) spatial density and velocity distributions. Moreover, we randomly generated one set, `s1`, of dimensionless spin vectors for the IMBHs ($\boldsymbol{\alpha}_i$, for $i = 1, 2, \ldots, N$) following a uniform distribution in a sphere of unitary radius. For both set 1 and set 2, we then performed a first subset of 10 simulations, called set 1A and 2A, with all spins equal to zero, and a second subset, named 1B and 2B, of 10 simulations each, where the spins are selected according to the procedure above. A sketch of the main parameters of the various simulations is given in Table 2.

To enhance accuracy in the computations, in the code we use R_0 as length unit and $M_{\rm tot} = M_{\rm S} + M_{\rm g}$ as mass unit, with $M_{\rm g}$ the galactic mass inside the sphere of radius R_0. The time unit $\mathrm{U_t}$ is chosen so as to ensure $G = 1$:

$$\mathrm{U_t} = \frac{R_0^{3/2}}{\sqrt{GM_{\rm tot}}} = \begin{cases}0.107\ \text{yr, for set 1,}\\ 3.365\ \text{yr, for set 2.}\end{cases} \tag{11}$$

The above time is, actually, the typical crossing time of the system. Due to the huge space density of the IMBH cluster under study, the dynamics is very violent and computationally demanding. Moreover, the computational cost of the planned simulations clearly varies as $\mathcal{O}(t_{\rm max}/\mathrm{U_t})$, so that, to integrate up to the same physical time $t_{\rm max}$, a simulation of set 1 would require, a priori, an ∼30 times longer (in terms of CPU time) simulation than one of set 2. Of course, many other issues have an impact on the computational speed, and indeed different simulations pertaining to the same set (1 or 2) proceeded at different speeds. Therefore, we decided to simulate the evolution of the system over 4000 $\mathrm{U_t}$ in each case, which means that for the denser configurations of set 1 we have $t_{\rm max} = 426$ yr while for set 2 we have $t_{\rm max} = 13\,462$ yr (that is a factor 31.6 in terms of physical time).

3.4 The actual role of the recoil velocity

For set 1, corresponding to the densest cluster, the rescaled initial velocities range from a few hundred km s^{-1} to ∼5400 km s^{-1}, with an average value $\langle v\rangle = 4012$ km s^{-1}. On the other hand, the recoil velocity after merger is at most 500 km s^{-1} (200 km s^{-1} on average), generally small with respect to the velocity of the CoM of the precursor binary and not large enough to overcome the escape velocity ($\simeq$7110 km s^{-1}). The two top panels of Fig. 4 (which refer to set 1) suggest that the recoil velocity alters the course of some of the individual trajectories, but it does not have, on average, a very significant impact on the overall evolution of the cluster.

In set 2, where the IMBHs are initially less densely packed, the initial velocities range from 100 to $\sim$1700 km s^{-1}, with average value $\langle v \rangle = 1270$ km s^{-1}. Due to the lower escape velocity, the recoil velocity is expected to have a more relevant impact on the course of the simulation than in set 1. Anyway, as shown in the two bottom panels of Fig. 4, the recoil velocity is still one order of magnitude smaller than both the progenitor binary CoM velocity and escape velocity this latter being $\simeq$2250 km s^{-1}. Therefore, it can rarely cause the ejection of a merger remnant from the main cluster by overcoming the local escape velocity. Note the decrease with time of both CoM and recoil velocity in both set 1 and set 2, explained by decreasing with time of q.

Because the effect of the recoil velocity is mostly negligible, there is no statistical difference, neither between the results of the subset 1A and 1B nor between the results of the subset 2A and 2B.

For this reason, in the rest of this work we will, as a rule, only present results averaged over the whole set 1 and the whole set 2, and not detailed subset's results.

3.5 The actual role of the external potential

As we said in Section 3, for our simulations, we emulate the central environment of the Milky Way by an external density profile that is the superposition of a Dehnen profile characterized by $M_{\rm D} = 10^{11}$ M$_\odot$, $r_{\rm D} = 2000$ pc, and $\gamma_{\rm D} = 0.1$ and a Plummer profile characterized by $M_{\rm P} = 2.5 \times 10^7$ M$_\odot$ and $r_{\rm P} = 3.2$ pc.

The galactic mass inside the sphere of radius R_0, $M_{\rm g}(R_0)$, is in both the sets of simulations very small with respect to the total mass in IMBHs ($M_{\rm g}/M_{\rm S} = 4.1 \times 10^{-11}$ for set 1 and 4.1×10^{-8} for set 2), so that the external field is altogether negligible in terms of gravitational acceleration with respect to the pairwise IMBH–IMBH gravitational acceleration. Moreover, for small distances r to the centre ($r \sim$ 1 mpc), the background density is dominated by the Plummer profile, which is flat for $r \ll r_{\rm P} = 3.2$ pc. Hence, for both sets of our simulations, the background density averaged within the sphere of radius R_0 has the same value $\langle \rho(< R_0) \rangle \simeq 1.8 \times 10^5$ M$_\odot$ pc^{-3}. We can estimate $\left\langle \sum_{1 \le i < j \le N} |\mathbf{r}_i - \mathbf{r}_j|^{-2} \right\rangle \simeq 3N/(4R_0^2)$, so that the initial effect of dynamical friction $\mathbf{f}_{\rm df}$ with respect to the Newtonian interactions $\mathbf{f}_N$ can be quantified as

$$\frac{|\mathbf{f}_{\rm df}|}{|\mathbf{f}_N|} \simeq 16\pi G \ln\Lambda \langle \rho(< R_0) \rangle \left\langle \frac{F(v/\sigma)}{v^2} \right\rangle \frac{R_0^2}{3N}, \qquad (12)$$

$$\simeq \begin{cases} 7.8 \times 10^{-12}, & \text{for set 1,} \\ 7.8 \times 10^{-9}, & \text{for set 2,} \end{cases}$$

which is totally negligible. Anyway, the role of external potential is relevant to determine the fate of objects that, during the various interactions and also after mergers, acquire a speed sufficient to move far from the centre. Most of them do not overcome the escape velocity and so make a fast return to the internal region due to the combined action (gravitational acceleration and dynamical friction) of the external field. This slows down the cluster dissolution.

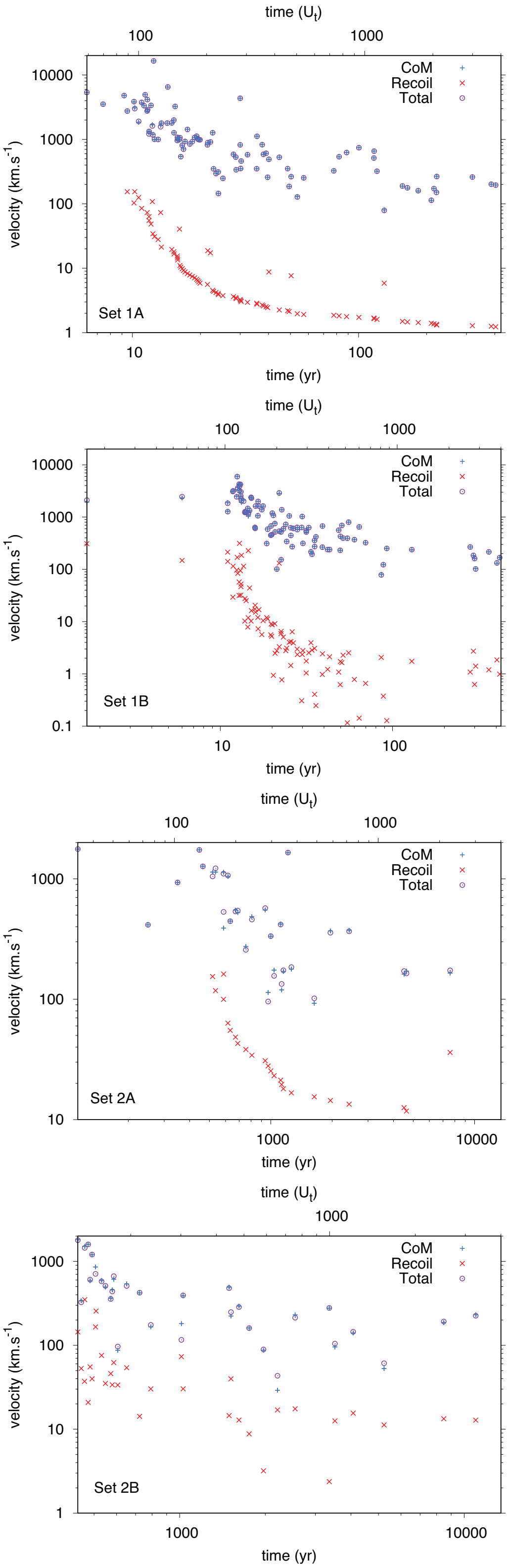

Figure 4. Contribution of the recoil velocity (in red) and progenitor binary CoM velocity (in blue) to the total velocity of the remnant (in purple) at each merger, over one simulation of each subset. From top to bottom: set 1A, set 1B, set 2A, and set 2B.

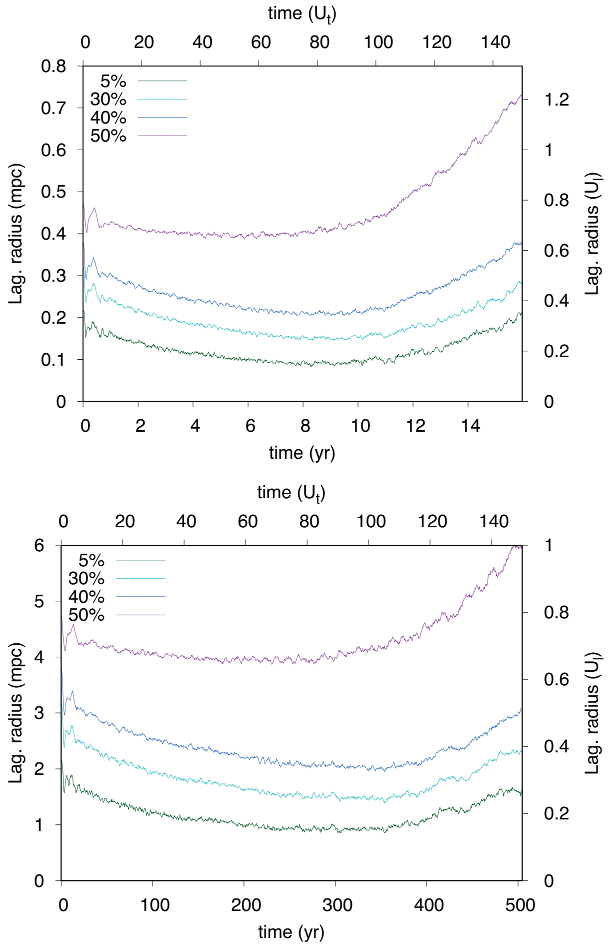

Figure 5. Initial evolution of the Lagrangian radii (from 5 per cent to 50 per cent) of the system, centred on the CoM of its bound core. Top: average over the 20 simulations of set 1. Bottom: average over the 20 simulations of set 2.

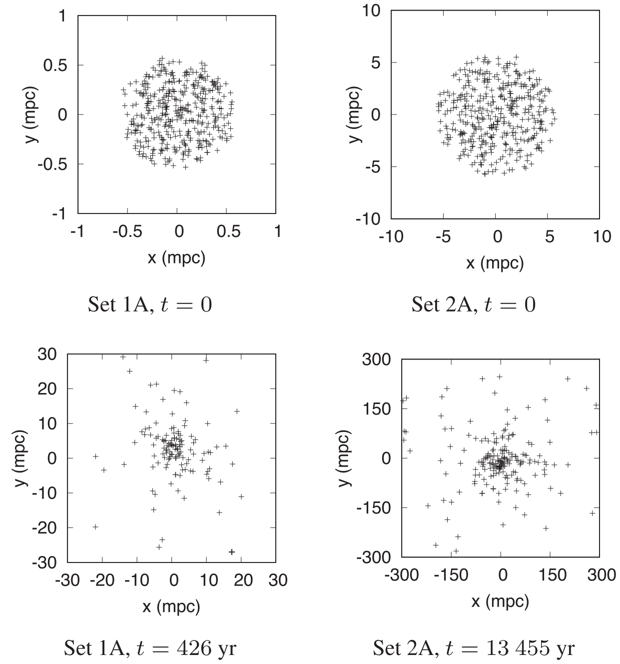

Figure 6 Snapshots of the stellar system at $t = 0$ and $t = t_{\max}$ for arbitrarily chosen simulations of set 1A and set 2A, centred on the CoM of the bound core of the system.

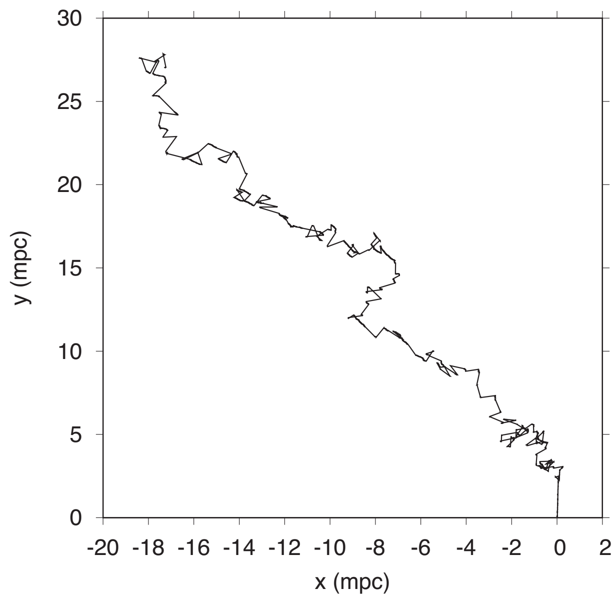

Figure 7. Drift along time of the CoM of the bound core with respect to the CoM of the whole system, for one of the simulations of set 1A.

4 RESULTS

Here, we present results for our sets of simulations, whose characteristics have been described in Section 3.3 and summarized in Table 2. Results are indicative of the overall fate of the superdense cluster of IMBHs and show the clear growth of an SMBH seed via subsequent merger events, each of them characterized by a burst of GW emission.

4.1 Overall evolution of the cluster

Fig. 5 displays the average (over all the simulations of set 1 and set 2, respectively) evolution of some of the Lagrangian radii of the system. In Fig. 5, we see that after a period of contraction lasting, in both cases, about 100 crossing times, the system expands steadily. The evolution leads to the substantial internal change characteristic of self-gravitating systems: An initial homogeneous distribution is remodelled into a dense core surrounded by a low-density halo. The snapshots of the system configurations on one of the coordinate planes in Fig. 6 give a qualitative sketch of this change in the layout of the system.

Note that, due to the non-isotropic expulsion of some IMBHs, the CoM of the actual cluster (that is the gravitationally bound part or 'core' of the system) deviates from the position of the CoM of the whole system (see Fig. 7). For a better display we, thus, decided to evaluate the Lagrangian radii with respect to the CoM of the bound core of the system. We defined this bound core of the cluster by excluding those objects that reach with positive energy a distance from the system such as to make very unlikely that they can undergo interactions able to lead them back to negative energy.

The Lagrangian radii are evaluated in percentage of the total mass of the cluster and so all the bodies, including possibly escaping IMBHs and growing (in mass) objects, are taken into account. Of course, the escaping IMBHs lead to a natural increase of the high-

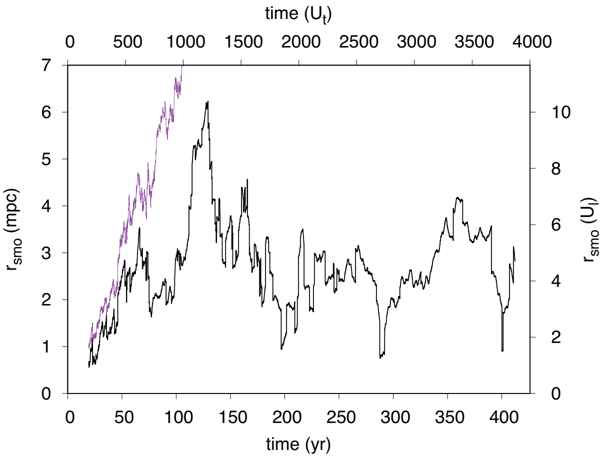

Figure 8. Black line gives the distance ($r_{\rm smo}$) of the growing supermassive object to the CoM of the bound 'core' of the system, for one arbitrarily chosen simulation of set 1A, taken as example. For comparison, we also give in purple the half-mass radius of the system. The curves are plotted starting from the time when the SMBH 'seed' is already grown by 42 IMBH mergers.

percentage Lagrangian radii so that in Fig. 5 we display only up to the 50 percent Lagrangian radius ($R_{1/2}$).

Note that growing massive objects, although they remain inside the bound core of the system and close to its CoM, do not a priori coincide with this CoM (see Fig. 8 that shows, also, how the growing BH movement is since the beginning well within the half-mass radius) and could, consequently, induce sharp variations in the latter evolution of the low-percentage Lagrangian radii.

The late time evolution of the average half-mass radius $R_{1/2}$ (50 percent Lagrangian radius), which is a good definition of the system radial scale, is well fitted by a linear relation:

$$R_{1/2}(t) \simeq a_{1/2}t + b_{1/2}. \tag{13}$$

For set 1 and $t > 15$ yr, the values of the parameters are

$$\begin{cases} a_{1/2} = 5.613 \times 10^{-2} \pm 3.10^{-5} \text{ mpc yr}^{-1}, \\ b_{1/2} = -0.012 \pm 0.009 \text{ mpc}, \end{cases} \tag{14}$$

leading to a root mean square error of the fit equal to 0.8 mpc for $R_{1/2}$. For set 2 and $t > 500$ yr, the values are

$$\begin{cases} a_{1/2} = 1.8070 \times 10^{-2} \pm 6.10^{-6} \text{ mpc yr}^{-1}, \\ b_{1/2} = -8.09 \pm 5.10^{-2} \text{ mpc}, \end{cases} \tag{15}$$

giving a root mean square error equal to 5 mpc.

The average half-mass radius at the final simulation time for set 1 is equal to 24 mpc (37 mpc for set 2), that is 50 times (8 times for set 2) the initial half-mass radius, $R_{1/2}(0) = 2^{-1/3}R_0$.

Even with our original safety margin of one order of magnitude for the initial cluster radial size, at the end of the simulation the core of the cluster extends much farther out than the area allowed for our purpose of mimicking the presence of an SMBH by a dense cluster of IMBHs. This is true for every simulation of set 1 and not only on average. This is even more the case for set 2, where no safety margin was taken. This result is not surprising: We actually expected that the extreme conditions required (a stable system of IMBHs of total mass $M_S = 4 \times 10^6\,\mathrm{M}_\odot$ and maximal size $\leq$5 mpc) were very unlikely to be reached.

As we see in the next section, in both set 1 and set 2 the IMBH cluster undergoes various merger episodes. This has relevant consequences, whose main result is the formation of a very massive BH as coming out from the dominant object growing up after successive merger events.

Hence, we conclude that, as expected on basic theoretical understanding, the answer to the first of the issues we raised in introduction is negative: A cluster of IMBHs dense enough to mimic the dynamical role of an SMBH would not be stable for a significant time. On the other hand, thanks to our simulations we saw how this instability of the system results in a quick aggregation of mass, efficient enough to beget an SMBH from successive mergers of less massive seeds.

4.2 The formation of an SMBH by subsequent mergers

Along the time evolution of the IMBH cluster under study, many merger events occur. Besides the relevance they have in both growing a supermassive object from the dominant aggregation seed and their repeated bursts of GWs, the merger events have an effect on the overall cluster structure

Actually, in our simulations the mechanical energy of the system varies due to two phenomena: one is the energy loss via gravitational radiation (accounted for by the 2.5-order PN terms in ARWV) during the binary inspiral, while the other is a consequence of collisions, in the way we explained in Section 3.2.

As we saw in Section 3.2, every merger corresponds to a small injection of positive energy in the system (equation 10) so that the total energy of the N-body system increases whenever a merger event takes place. As a matter of fact, the total mechanical energy we compute all along our simulations shows a stepwise increase after every merger event (see Fig. 9). After numerous successive merger events, the total energy can eventually become positive, so that the system becomes gravitationally unbound.

In extremely dense systems such as the ones studied here, close three-body encounters are found to happen often, causing binary pairs to form and tighten, ultimately leading to merger through relativistic final orbital decay. As we mentioned in Section 3.1, ARWV is specifically designed to account for these situations, at least until PN approximation maintains its validity.

As Fig. 10 shows, the merger rate comes to a peak at about 100 U_t after the beginning of the simulation for both set 1 and set 2 (in physical time, it is $t \simeq 10$ yr for set 1 and $t \simeq 500$ yr for set 2). This peak time corresponds to the time of maximum compression of the IMBH cluster, as seen in Fig. 5. The merger remnants, if not ejected from the core of the cluster due to high recoil velocity (which, as we have already shown, is a very rare case), constitute an aggregation seed apt to induce further mergers. At this time, the number of merger remnants is maximal (see Table 3 for more details).

These remnants merge among themselves rather quickly, leading to a dominant very massive object sitting almost at the centre of the potential well and 'absorbing' other bodies. Later, due to the contemporary effects of the expansion of the cluster as a whole and the progressive depletion of IMBHs (many of them having been already captured), the merger rate drops and, so, the mass-aggregation process nearly comes to an end (see Fig. 11).

For set 1, the average number of merger events occurring in 426 yr is 93.05. On average, only three actual merger remnants survived in the cluster at the end of the simulation, one of which contains almost all the mass aggregated. The mass of this supermassive remnant amounts on average to 23 per cent of the total initial mass of the system, that is, indeed, 23 per cent of the mass of the SMBH at the centre of the Milky Way. A rough and not completely reliable extrapolation of this result says that an initial number of IMBHs 4.35 larger (i.e. 1740 IMBHs of $10^4\,\mathrm{M}_\odot$ each) would be needed to grow an SMBH of $4 \times 10^6\,\mathrm{M}_\odot$.

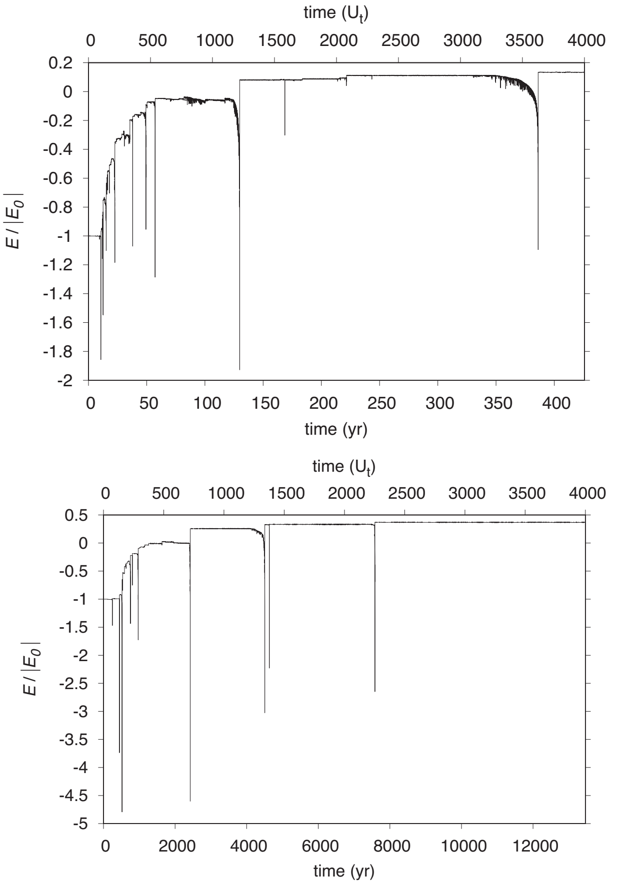

Figure 9. Evolution of the total mechanical energy E of the system along time, in fraction of its absolute initial value $|E_0|$. Top: a simulation of set 1A. Bottom: a simulation of set 2A.

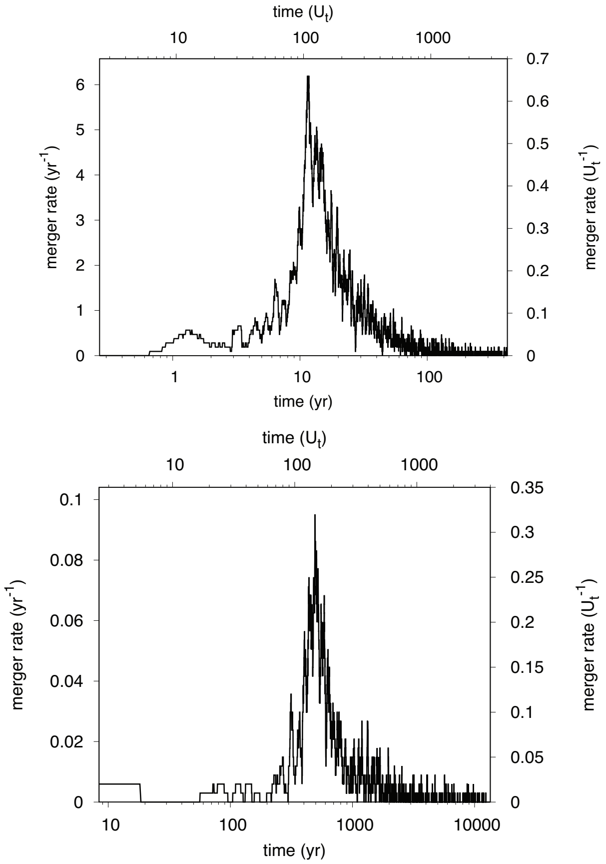

Figure 10. Top panel: average rate of merger over the 20 simulations of set 1. Bottom panel: average rate of merger over the 20 simulations of set 2.

Table 3. Minimal, maximal, and average (over all simulations of the indicated set) fraction of the total mass M_S gone into merger remnants at the time when the merging rate is maximum.

	Peak time	Min.	Max.	Average
Set 1A	11.45 yr	0.005	0.045	0.0235
Set 1B	11.04 yr	0.005	0.05	0.0205
Set 2A	494.46 yr	0.01	0.025	0.0175
Set 2B	493.95 yr	0.005	0.0338	0.0139

For set 2, the dynamics is less violent, as shown by that the maximal number of contemporary merger remnants is much smaller. During 13 455 yr, an average of 33.9 merger events happened, leading to the survival of only 2 remnants, one of which accumulated the mass of 33.95 initial bodies (that is, 8.5 per cent of the total mass of the system).

These are interesting results, because they state the possibility to grow a very massive BH by the violent interactive dynamics of a set of densely packed IMBHs.

We already said that the initial conditions of our system are not the most realistic and that a better modelization (with less extreme hypotheses) should be considered in a further investigation. This new model would likely lead to a smaller rate of mass accretion, as hinted by the fact that set 2, whose initial spatial distribution was extended in radial size for a factor 10 with respect to set 1, shows an approximately 10 times lesser rate of accretion. However, what is really interesting in our present results is that, even if this rate were to decrease by two or even three order of magnitude, a comparable fraction of the BH mass would be aggregated in less than one million years.

4.3 GWs from IMBH mergers

Let $\dot{E}_{\rm GW} \geq 0$ denote the energy radiated away by GW per unit of time (emitted power), so that $E_{\rm GW}(t) = \int_0^t \dot{E}_{\rm GW}\, {\rm d}t$ is the energy lost by the system from the beginning of the simulation up to time t. Proper unit of measure for the energy loss is the absolute value of the initial gravitational (binding) energy $|\Omega_0|$ of the system, so that we express $\dot{E}_{\rm GW}$ either in units of $|\Omega_0|$ yr^{-1} or in units of $|\Omega_0|$ U$_{\rm t}^{-1}$.

In set 1, the magnitude of the peak in power emission preceding each merger ranges from $\dot{E}_{\rm GW} \sim 10^{-13}\, |\Omega_0|$ yr^{-1} to $\dot{E}_{\rm GW} = 0.6\, |\Omega_0|$ yr^{-1}, for all 20 simulations. In set 2, it ranges from $\dot{E}_{\rm GW} \sim 10^{-13}\, |\Omega_0|$ yr^{-1} to $\dot{E}_{\rm GW} = 8.3\, |\Omega_0|$ yr^{-1}, for all 20 simulations.

Most of the merger events occur relatively soon after the beginning of the simulation, when the system is still very dense. Prior to the merger, the two progenitor bodies form a loose binary that is subjected to repeated successive interactions with other IMBHs. At a later stage of its orbital shrinking, the binary starts emitting GWs until it, eventually, merges.

It is notable that while the evolution of binaries formed along the way shows a quite erratic semimajor axis versus eccentricity behaviour due to significant external perturbations, when the semi-major axis has shrunk enough (and the eccentricity reached a high value) the final evolution down to the merger resembles, at least for

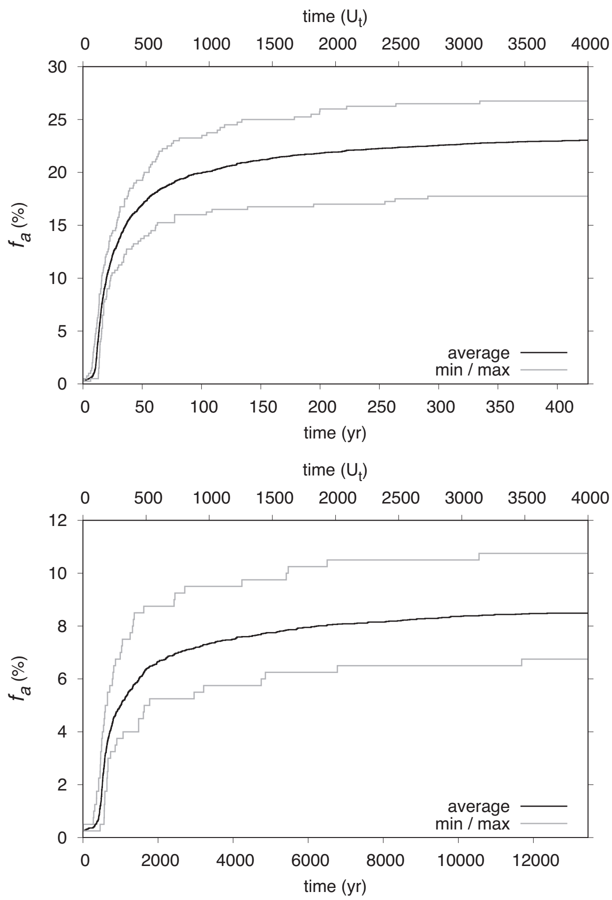

Figure 11. Percentage, f_a, of the stellar mass accumulated into one single body along the simulation. Top: Average over the 20 simulations of set 1. Bottom: Average over the 20 simulations of set 2.

what can be seen by the limited output time resolution of our *N*-body simulations, to that expected in isolation. This is clearly shown in Fig. 12, where the top panel plots a versus e for three sample cases of binaries in set 2A that undergo a merger. The characteristics of the three binary systems undergoing merger are given in Table 4, where the 'initial' semimajor axis and eccentricity (a_0 and e_0) are corresponding to those labelled with a '+' symbol in panel (a) of Fig. 12. The oscillations in the a versus e relation are caused by passing-by object perturbations, until ('+' symbols in Fig. 12a) the binaries are tight and eccentric enough to evolve independently of the external field. This phase, which leads to the final merger due to GW energy loss, is followed in the ARWV output until the 'x' symbols. The whole evolution until merging reported in Fig. 12(b) is obtained, instead, by integration of equations 5.6 and 5.7 in Peters (1964). Notably, the times to merger as obtained by ARWV and by the Peters-like integrations differ by less than 6 per cent. For the sake of clarity and comparison, the bottom panel of Fig. 12 gives the a versus e evolution computed by integrating the above-mentioned evolutive differential equations from Peters (1964), with initial conditions taken as the ones corresponding to the three '+' symbols marked in Fig. 12(a).

In the first case of Table 4, the two progenitors are basic $10^4\,\mathrm{M}_\odot$ BHs. In the second, the two progenitors are small merger remnants of mass $2 \times 10^4\,\mathrm{M}_\odot$. Thus, in both cases the mass ratio is equal to 1. These two mergers occur relatively soon after the beginning of the

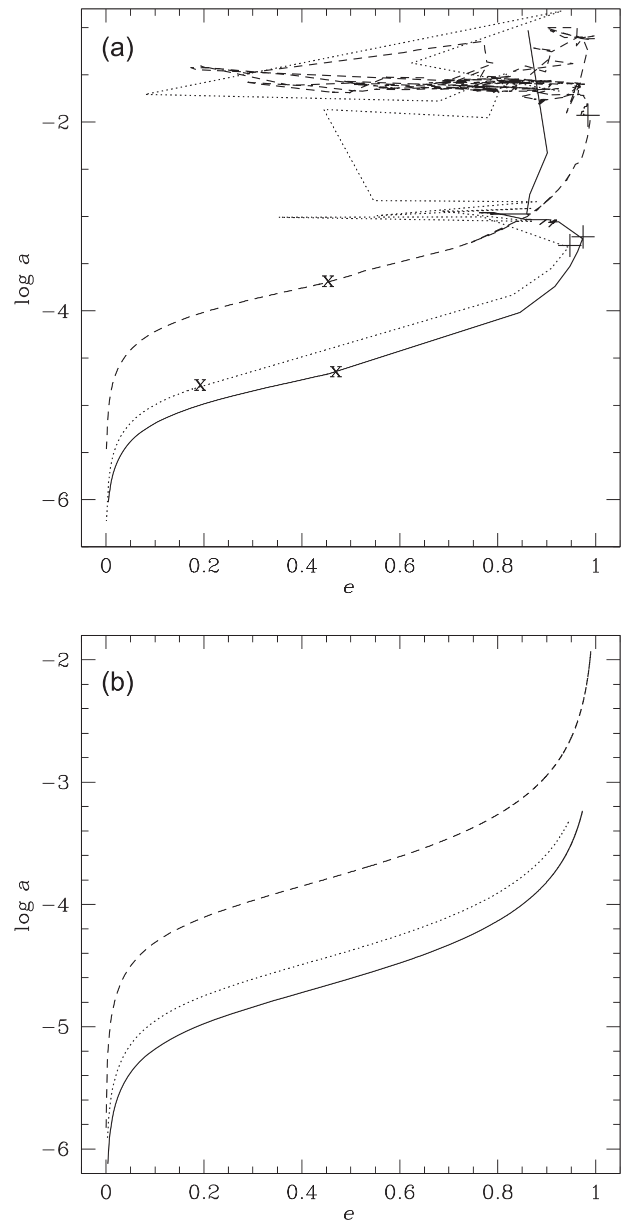

Figure 12. Top panel (a): semimajor axis (in units of U_l) versus eccentricity evolution for three binaries pertaining to the same simulation of set 2A. The '+' symbols mark the beginning of the GW-dominated phase. The 'x' symbols mark the last ARWV output before the merger (see the text). Bottom panel (b): a versus e final evolution according to Peters (1964) equations, with initial conditions corresponding to the three '+' markers in the top panel. Solid line: case 1; dotted line: case 2; dashed line: case 3.

Table 4. For the three cases (as labelled in column 1): masses in $10^4\,\mathrm{M}_\odot$ (columns 2 and 3), mass ratio (column 4), initial semimajor axis (in au) and eccentricity (columns 5 and 6), merger time in U_t (column 7), and fraction of GW energy released with respect to the rest energy ($m = m_1 + m_2$) (column 8).

Case	m_1	m_2	q	a_0	e_0	t_m	$E_{GW}/(mc^2)$
1	1	1	1	0.72	0.97	74.21	0.36
2	2	2	1	0.58	0.94	132.60	0.049
3	2	29	0.069	14.5	0.99	2252.98	0.021

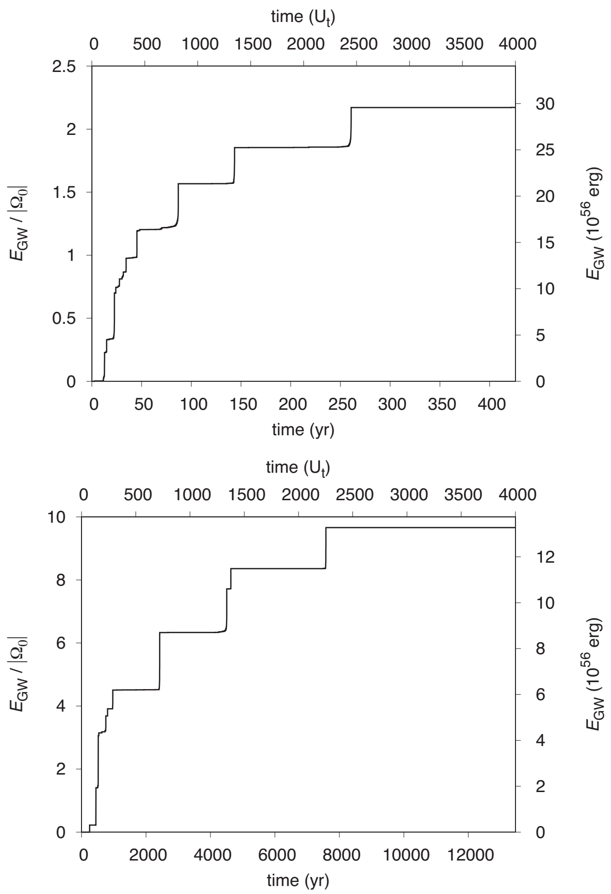

Figure 13. Energy emitted by the system throughout its evolution, for one of the simulations of set 1A (top) and one of set 2A (bottom).

simulation (t_m = 74.21 and 132.6 U_t), when the system is still very dense.

In the third case, one of the objects in the binary is the growing SMBH and the other a small remnant of a previous merger, giving a mass ratio of 29:2. This merger occurs later in the simulation (t_m = 2252.98 U_t), when the system has largely expanded. The bodies involved in this merger are inside a region where the density is three orders of magnitude less than that in the two other considered merger cases. Thus, the encounters with passing-by objects are much less frequent and some phases of the process (loose binary → tight binary emitting GW → merger) last longer. In this case, the GW emission phase extends over 16.8 yr, which is 5 times longer than the GW emission of the two other merger events displayed in Fig. 12 (mainly because of the significantly larger a_0 in spite of larger masses and slightly larger e_0) with a peak intensity at 2.2 $|\Omega_0|$ yr^{-1} and a half-power decay time of 7.8 d.

Fig. 13 displays an example of the evolution over time of the amount of energy lost by GW, E_{GW}, in one arbitrary chosen simulation of set 1A (upper panel) and of set 2A (lower panel). The total energy lost by the system at the end of this simulation is equal to 2.56 $|\Omega_0|$ for the set 1 case and 9.66 $|\Omega_0|$ for the set 2 case. Due to the different initial compactness of the two simulated systems, the dynamics of set 1 case is faster, explaining why at the same physical time of 426 yr (end of set 1's simulations) the GW energy released for set 1 overwhelms that of set 2 case. On the other side, the set 2 case shows a progressive significant GW emission at later times, so that the average time rate of GW emission is not so different in the two cases. If we analyse the output in terms of the characteristic time unit, then in 4000 U_t the set 2 simulation emits on average 4 times more energy in terms of Ω_0, but 2 times less in absolute value.

For set 1, the average (over the 20 simulations) quantity of energy lost by the system after 426 yr is equal to 2.32 $|\Omega_0|$. This corresponds to the conversion of 0.082 per cent of the initial total mass into energy, a little less than 1/3 of the initial individual IMBH mass.

For set 2, the average (over the 20 simulations) quantity of energy lost by the system after 13 455 yr is equal to 6.09 $|\Omega_0|$. This corresponds to the conversion of 0.012 per cent of the initial total mass into energy, a little less than 1/20 of the initial individual IMBH mass.

5 CONCLUSIONS

In this paper, we studied the possible fate of a set of IMBHs that have allegedly been transported to the Galactic Centre by their hosting massive star clusters. The possible mechanism of transport and confinement to the central Galactic region has been identified as due to dynamical friction braking of the star background on the motion of massive GCs hosting IMBHs.

We followed the violent dynamics of this superdense cluster of IMBHs (400 IMBHs of mass 10^4 $M_\odot$ each, to give a total mass ~ equal to the one estimated for the Sgr A* putative BH) with a high-precision *N*-body integrator (ARWV; see Chassonnery et al. 2019) containing an accurate treatment of close encounters and of general relativistic effects in the PN approximation scheme. We chose two different initial concentrations for the IMBH cluster and included an accurate treatment of recoil velocity after merger following modern GR prescriptions.

Our findings are as follows:

(i) the superdense cluster evolves very fast, without reaching an equilibrium because of the contemporary effect of interactions leading to the expulsion of members and the onset of merger events;

(ii) the relativistic recoil velocity is rarely high enough to overcome the escape speed, mainly due to that the initial mass ratio, q, of the IMBH is $q = 1$;

(iii) with different efficiency in dependence on the initial number density of the simulated clusters of IMBHs, merger events lead to a dominant 'aggregation' seed that can grow up in mass to more than 20 per cent of the initial mass of the cluster;

(iv) after this quick growth of what is, actually, an SMBH, the accretion phenomenon slows down due to the dispersal of the residual cluster that makes the further merger cross-section exceedingly small;

(v) a simple scaling of our numerical results for the more compact initial cluster considered indicates that a cluster of 1800 IMBHs with a radius <1 mpc could lead to the formation of an SMBH of the mass of Sgr A*;

(vi) the various mergers, both before and after the onset of a dominant aggregation SMBH seed, generate GWs, whose radiated energy is accounted for by the 2.5 order terms in the PN approximation. The mergers start as equal-mass merger and proceed towards the regime of IMRIs (intermediate-mass ratio inspirals, $m_2/m_1 \sim 100$), and the merging masses are so large that the GW output is peaked at very low frequencies (<1 Hz). The frequency of the emission peak decreases with growing merger mass, such that to make them undetectable from ground but still a very appealing source for future space antennas like the joint ESA–NASA satellite interferometer LISA (https://sci.esa.int/web/lisa and http://lisa.jpl.nasa.gov/).

(vii) the overall evolution of the studied systems, as well the rate of growth of the SMBH, is negligibly influenced by the individual IMBH spin because of the low value of the recoil velocity after merger with respect to the local escape velocity.

This work will be generalized to a more likely framework of IMBHs that are not considered as ab initio packed in a narrow region around the Galactic Centre but that fall progressively there, where they start interacting among themselves.

ACKNOWLEDGEMENTS

We acknowledge support by the Amaldi Research Center (Sapienza, Università di Roma, I) funded by the MIUR programme 'Dipartimento di Eccellenza' (CUP: B81I18001170001). We thank Seppo Mikkola for his help in the use and modifications of the ARWV code. P.C. also thanks the Department of Physics of Sapienza (Università di Roma, I) for the hospitality during the preparation of this work. A warm thanks is also due to R. Schneider for her support during the academic stage of P. C. at Sapienza (Università di Roma, I).

Finally, we thank an anonymous referee for specific comments that helped in the presentation of the paper results.

DATA AVAILABILITY

The data output of this article will be shared on reasonable request to the corresponding author and is subjected to proper acknowledgement to this paper.

REFERENCES

Aarseth S. J., 1999, PASP, 111, 1333
Agarwal M., Milosavljević M., 2011, ApJ, 729, 35
Antonini F., Capuzzo-Dolcetta R., Mastrobuono-Battisti A., Merritt D., 2012, ApJ, 750, 111
Antonini F., Gieles M., Gualandris A., 2019, MNRAS, 486, 5008
Arca-Sedda M., Capuzzo-Dolcetta R., 2014a, ApJ, 785, 51
Arca-Sedda M., Capuzzo-Dolcetta R., 2014b, MNRAS, 444, 3738
Arca-Sedda M., Capuzzo-Dolcetta R., 2017, MNRAS, 471, 478
Begelman M. C., Rees M. J., 1978, MNRAS, 185, 847
Boehle A. et al., 2016, ApJ, 830, 17
Capuzzo-Dolcetta R., 1993, ApJ, 415, 616
Capuzzo-Dolcetta R., Vicari A., 2005, MNRAS, 356, 899
Chandrasekhar S., 1943, ApJ, 97, 255
Chassonnery P., Capuzzo-Dolcetta R., Mikkola S., 2019, preprint (arXiv:1910.05202)
Dehnen W., 1993, MNRAS, 265, 250
de Sitter W., 1916, MNRAS, 77, 155
Event Horizon Telescope Collaboration, 2019, ApJ, 875, L1
Ghez A. M., Salim S., Hornstein S. D., Tanner A., Lu J. R., Morris M., Becklin E. E., Duchene G., 2005, ApJ, 620, 744
Gillessen S., Eisenhauer F., Trippe S., Alexander T., Genzel R., Martins F., Ott T., 2009, ApJ, 692, 1075
GRAVITY Collaboration, 2018, A&A, 615, L15
GRAVITY Collaboration, 2020, A&A, 636, L5
Healy J., Lousto C. O., 2018, Phys. Rev. D, 97, 084002
Healy J., Lousto C. O., Zlochower Y., 2014, Phys. Rev. D, 90, 104004
Healy J., Lousto C. O., Zlochower Y., 2017, Phys. Rev. D, 96, 024031
Hellström C., Mikkola S., 2010, Celest. Mech. Dyn. Astron., 106, 143
Kroupa P., Subr L., Jerabkova T., Wang L., 2020, MNRAS, 498, 5652
Kupi G., Amaro-Seoane P., Spurzem R., 2006, MNRAS, 371, L45
Lightman A. P., Fall S. M., 1978, ApJ, 221, 567
Memmesheimer R.-M., Gopakumar A., Schäfer G., 2004, Phys. Rev. D, 70, 104011
Merritt D., 2013, Dynamics and Evolution of Galactic Nuclei. Princeton Univ. Press, Princeton, NJ
Mikkola S., Aarseth S., 2002, Celest. Mech. Dyn. Astron., 84, 343
Mikkola S., Merritt D., 2008, AJ, 135, 2398
Mikkola S., Tanikawa K., 1999a, Celest. Mech. Dyn. Astron., 74, 287
Mikkola S., Tanikawa K., 1999b, MNRAS, 310, 745
Neumayer N., Seth A., Böker T., 2020, A&AR, 28, 4
Ostriker J. P., Binney J., Saha P., 1989, MNRAS, 241, 849
Pesce E., Capuzzo-Dolcetta R., Vietri M., 1992, MNRAS, 254, 466
Peters P. C., 1964, Phys. Rev., 136, 1224
Plummer H. C., 1911, MNRAS, 71, 460
Schartmann M., Burkert A., Ballone A., 2018, A&A, 616, L8
Schödel R., Feldmeier A., Kunneriath D., Stolovy S., Neumayer N., Amaro-Seoane P., Nishiyama S., 2014, A&A, 566, A47
Schutte Z., Reines A. E., Greene J. E., 2019, ApJ, 887, 245
Spitzer Lyman J., Hart M. H., 1971, ApJ, 164, 399
Spitzer Lyman J., Saslaw W. C., 1966, ApJ, 143, 400
Spitzer Lyman J., Stone M. E., 1967, ApJ, 147, 519
Spurzem R., 1999, J. Comput. Appl. Math., 109, 407
Tremaine S. D., Ostriker J. P., Spitzer L. J., 1975, ApJ, 196, 407

This paper has been typeset from a TEX/LATEX file prepared by the author.